Available online at www.sciencedirect.com
ScienceDirect
Tectonophysics 426 (2006) 135–152
TECTONOPHYSICS
www.elsevier.com/locate/tecto

The Gibraltar Arc seismogenic zone (part 1): Constraints on a shallow east dipping fault plane source for the 1755 Lisbon earthquake provided by seismic data, gravity and thermal modeling

Emmanuelle Thiebot, Marc-André Gutscher *

IUEM, Univ. Brest, UMR 6538, Plouzané, France

Accepted 7 February 2006
Available online 10 July 2006

Abstract

The Great Lisbon earthquake of 1755 with an estimated magnitude of 8.5–9.0 is the most destructive earthquake in European history, yet the source region remains enigmatic. Recent geophysical data provide compelling evidence for an active east dipping subduction zone beneath the nearby Gibraltar Arc. Marine seismic data in the Gulf of Cadiz image active thrust faults in an accretionary wedge, above an east dipping decollement and an eastward dipping basement. Tomographic and other data support subduction and rollback of a narrow slab of oceanic lithosphere beneath the westward advancing Gibraltar block.

Although, no instrumentally recorded seismicity has been documented for the subduction interface, we propose the hypothesis that this shallow east dipping fault plane is locked and capable of generating great earthquakes (like the Nankai or Cascadia seismogenic zones). We further propose this east dipping fault plane to be a candidate source for the Great Lisbon earthquake of 1755. In this paper we use all available geophysical data on the deep structure of the Gulf of Cadiz–Gibraltar region for the purpose of constraining the 3-D geometry of this potentially seismogenic fault plane. To this end, we use new depth processed seismic data, have interpreted all available published and unpublished time sections, examine the distribution of hypocenters and perform 2-D gravity modeling. Finally, a finite-element model of the forearc thermal structure is constructed to determine the temperature distribution along the fault interface and thus the thermally predicted updip and downdip limits of the seismogenic zone.

Keywords: Great Lisbon earthquake; Iberia; Morocco; Subduction; Seismic profiles; Thermal modeling

1. Introduction

The Great Lisbon earthquake of 1755 is the most destructive earthquake in European history, with an estimated magnitude of 8.5–9.0 (Martinez-Solares et al., 1979; Johnston, 1996) (Fig. 1). Yet, the tectonic source of this earthquake, which caused tens of thousands of deaths and triggered a devastating tsunami along the coasts of Southwest Iberia and Northwest Morocco, remains unknown to this day (Baptista et al., 1998; Gutscher, 2004). Several authors have recently proposed one or more basement highs at the SW extremity of the

* Corresponding author. Tel.: +33 2 98 49 87 27; fax: +33 2 98 49 87 60.
E-mail address: gutscher@univ-brest.fr (M.-A. Gutscher).

0040-1951/$ - see front matter © 2006 Elsevier B.V. All rights reserved.
doi:10.1016/j.tecto.2006.02.024

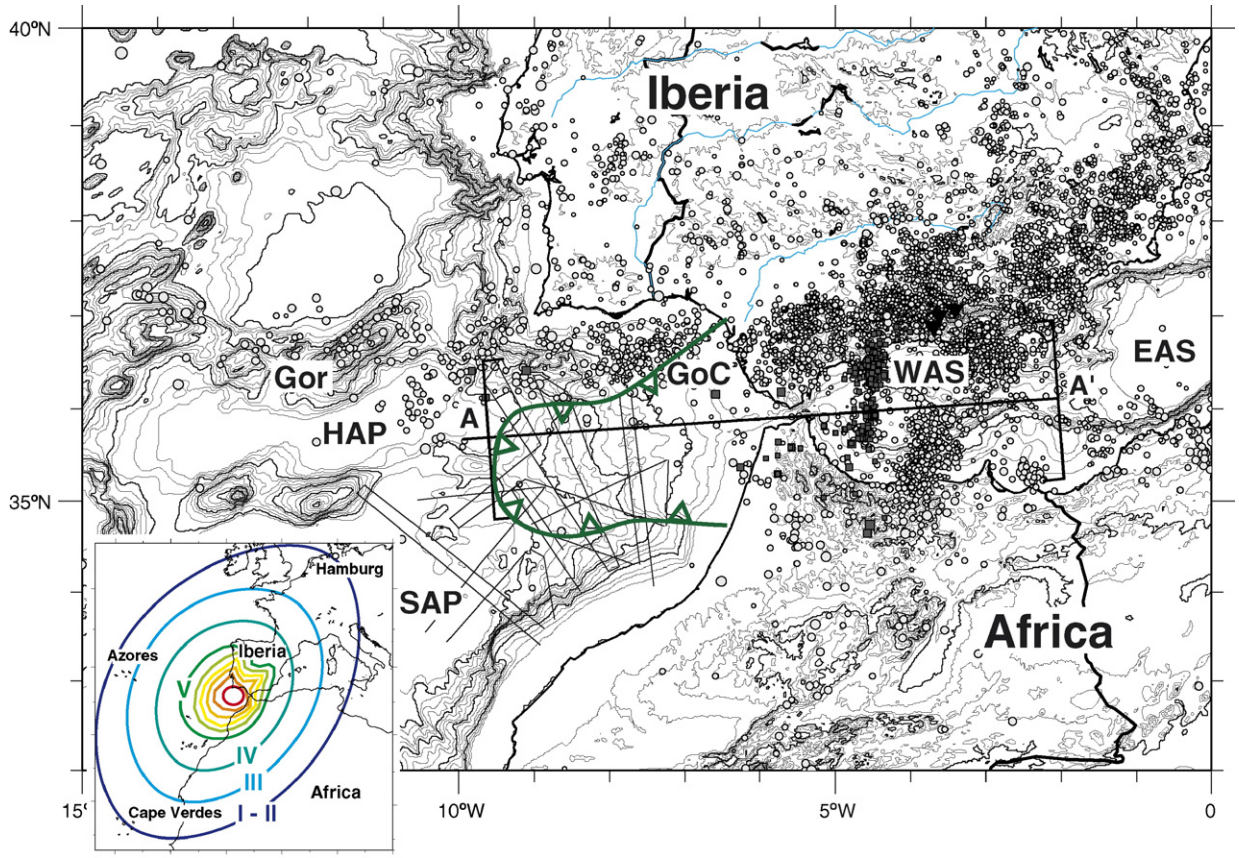

Fig. 1. General location map with bathymetric contours from GEBCO Digital Atlas (IOC et al., 2003), with a contour interval of 250 m and every 1000 m in bold. The position of the SISMAR network of seismic reflection profiles is indicated as well as the distribution of earthquake hypocenters for the period 1973–2003 (NEIC PDE Catalog) (light shaded circles represent hypocenter depth of 0–70 km; dark shaded squares represent hypocenter depths of 71–150 km; black triangles represent hypocenter depths of 600–660 km). The sampling box is shown for seismicity cross-section A–A′ (Fig. 2), as well as for the gravity model (Fig. 8) and the thermal model (Figs. 9 and 10). Gor=Gorringe Bank, HAP=Horseshoe Abyssal Plain, SAP=Seine Abyssal Plain, GoC=Gulf of Cadiz, WAS=West Alboran Sea, EAS=East Alboran Sea. Inset shows felt area of 1755 earthquake in NW Africa, western Europe and the NE Atlantic.

SW Iberian Margin to be the source of the 1755 earthquake (Zitellini et al., 2001; Terrinha et al., 2003; Gracia et al., 2003a,b). However, the structures proposed appear to be too small to generate an event of this great magnitude (M>8.5). The source region off SW Iberia is located at the eastern end of the portion of the Africa–Eurasia plate boundary commonly referred to as the Azores–Gibraltar transform (Sartori et al., 1994; Tortella et al., 1997; Jimenez-Munt et al., 2001). In Southern Iberia, the plate boundary is not clearly defined and encompasses a broad region of deformation at least 200 km wide (in a N–S direction) marked by moderately high seismicity (Preliminary Determination of Earthquakes (PDE) Catalog 1973−present; Negredo et al., 2002; Stich et al., 2003) (Fig. 1). Present-day plate convergence between Africa and Eurasia here is slow, only 4 mm/a along a NW–SE vector (Argus et al., 1989). However, plate kinematic reconstructions of the evolution of the adjacent Western Mediterranean region indicate periods of rapid micro-plate movement and subduction from the Oligocene to present (Rehault et al., 1985; Lonergan and White, 1997; Faccenna et al., 2001). Subduction of Tethyan oceanic lithosphere beneath the SW margin of Europe, led to back-arc rifting and locally, to sea-floor spreading and provoked large scale rotation and migration of Alpine crystalline massifs to present day positions in Calabria, the Kabylies and the Betic–Rif belt.

The arcuate Betic–Rif orogen is comprised of internal Alpine crystalline units and Eocene and younger allocthonous units with NW and SW vergent thrust nappes. This “Gibraltar” arc is non-volcanic and surrounds the West Alboran Sea, a region where strong Neogene subsidence occurred co-evally during westward

nappe transport (Lonergan and White, 1997). Miocene and older calc–alkaline volcanism is scattered across the West Alboran Sea. The geodynamics of this region has been interpreted in terms of east dipping subduction (Royden, 1993; Lonergan and White, 1997), though many alternate models exist. Geochemical studies of Alboran Sea magmatic rocks indicate subduction volcanism occurred here until at least Miocene times (Duggen et al., 2003, 2004). Recent marine geophysical data, combined with tomographic images, provide compelling evidence for current activity of a small eastward dipping subduction system beneath the Gibraltar Arc, driven by sinking and rollback of the slab to the west. Seismic reflection profiles and wide-angle profiles in the Gulf of Cadiz document an accretionary wedge, with active thrust faults soling out to an east dipping decollement and overlying an eastward dipping basement (Gutscher et al., 2002). The discovery of active mud volcanoes throughout the accretionary wedge lends further support to the interpretation of currently active subduction (Pinheiro et al., 2003).

Here, we explore the hypothesis that the active subduction zone represents a possible source region for the 1755 earthquake (Gutscher, 2004). Thus, we first investigate the 3-D geometry of the shallow east dipping fault plane associated with the Gibraltar subduction system (Fig. 2). We present new depth processed seismic data as well as a combined interpretation of all available seismic profiles in order to determine the shallow geometry (<20 km) of the fault plane. We use gravity modeling and the distribution of hypocenters, together with tomographic cross sections to determine the deeper geometry (>20 km). Finally, we construct a thermal model for the entire Gibraltar forearc and back-arc (the Alboran Sea) in order to determine the temperature distribution along the fault plane and thereby ascertain the likely updip and downdip limits of the potentially seismogenic zone.

2. Seismic data and geometry of the subduction fault plane

The geometry of the subduction fault plane is constrained by a network of deep seismic reflection profiles (Fig. 3). The multi-channel seismic (MCS) profiles were acquired during the SISMAR cruise, by R/V Nadir in April 2001, with a 360 channel, 4.5 km long streamer and a 4805 cu in tuned airgun array. Shot spacing ranged from 75 m (for purely MCS profiles) to 150 m (for joint OBS and MCS profiles). This provided 30- and 15-fold CDP coverage, respectively. Thus, CDP spacing was 6.25 m for the MCS only profiles and 12.5 m for the joint profiles. The sampling rate was 4 ms in all cases. Information on acquisition and processing of SISMAR MCS data are also available for profile SIS-4 further SW along the Moroccan continental margin (Contrucci et al., 2004), which was depth processed at the Geomar Seismic Processing Center.

MCS profiles SIS-16 and SIS-22 (Figs. 4 and 5) were pre-stack depth migrated at the Geomar Seismic Processing Center. The processing sequence included several steps. First a standard sequence was applied including static correction, time and space variant, band pass frequency filters, and a spherical divergence correction. Next a minimum delay transformation was

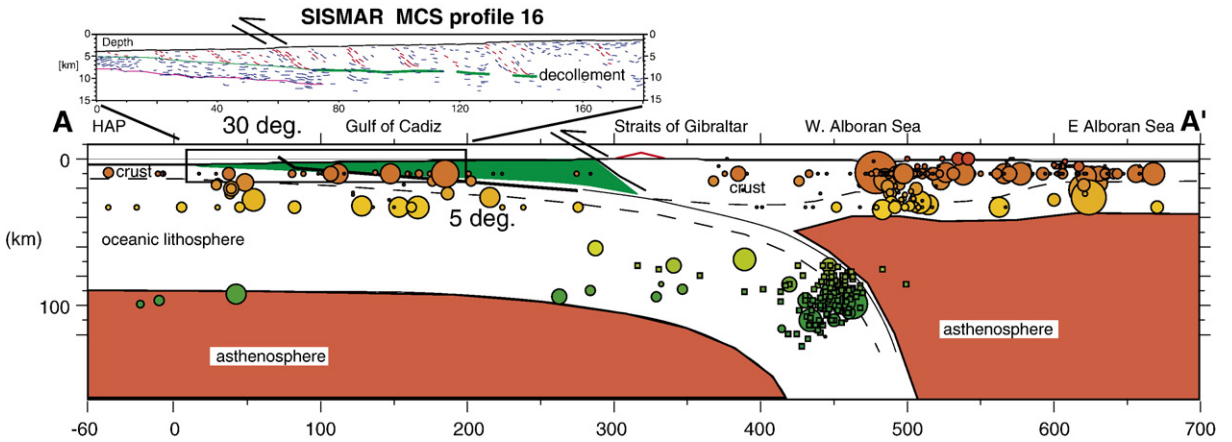

Fig. 2. Simplified lithospheric cross-section showing the geometry of the east dipping fault plane between the subducting slab and the upper plate (Gibraltar block) with the distribution of earthquake hypocenters (see Fig. 1 for sampling box). A simplified line drawing of SISMAR seismic profile 16 is projected onto the cross-section. The profile samples the frontal most portion of the fault plane.

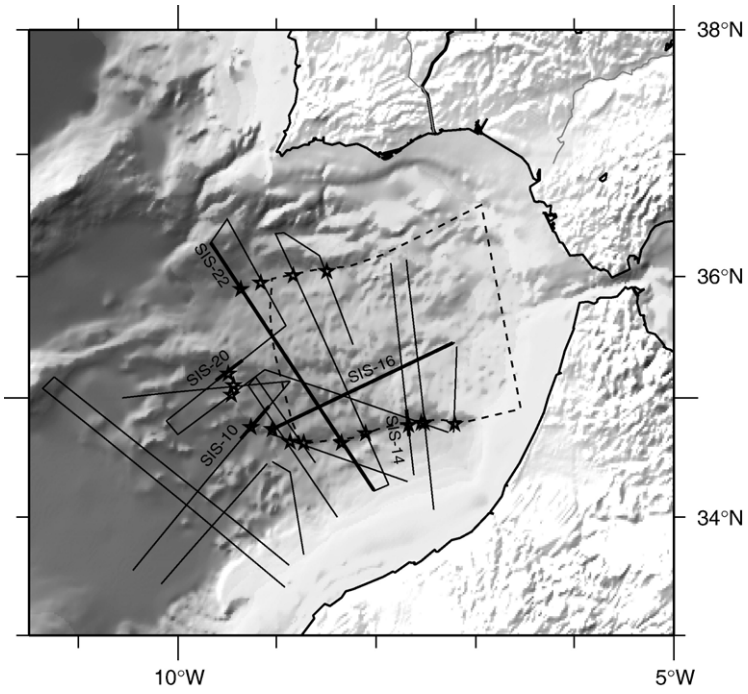

Fig. 3. Simplified location map with the network of SISMAR MCS profiles shown. Seismic sections shown in Figs. 4–6 are indicated by bold lines. The position of the deformation front of the westward vergent accretionary wedge in the Gulf of Cadiz is marked by stars. The lateral extent of the potentially seismogenic subduction fault plane is indicated by the dashed line.

applied. This was necessary because the airgun array was tuned to single-bubble mode (not minimum phase) and in order to apply deconvolution, the source wavelet must be minimum phase. Deconvolution was then performed to reduce the bubble reverberations (ringing). Inner trace muting and f–k filtering were applied in order to attenuate the multiple. Thereafter, a velocity model was constructed iteratively by focusing analysis, layer by layer, with a Kirchoff depth migration performed in between each subsequent step. Velocity analysis and depth migration were performed with the SIRIUS Software Package. Descriptions of the standard depth processing sequence may also be found in Flueh et al. (1998). The final, detailed velocity model was used for pre-stack depth migration and results in the true depth structural images shown in Figs. 4 and 5.

SIS-16 crosses the accretionary wedge approximately perpendicular to the deformation front, and parallel to the WSW tectonic transport direction, sampling roughly the frontal half of the potentially seismogenic fault plane (Fig. 4). OBS instruments deployed on this line, offer independent control on the depth to major crustal interfaces (top basement, Moho) (Gutscher et al., 2002). The depth migrated MCS profile images east dipping ramp thrusts soling out to a shallow east dipping decollement, as well as the eastward dipping sediment–basement interface (Fig. 4). As the frontal-most portion of an accretionary wedge is considered to deform aseismically (Byrne et al., 1988), it is likely that any co-seismic displacement may propagate along one of the prominent ramp thrusts. These ramp thrusts (sometimes called splay faults), typically have a dip of 30°–35° and are associated with 200–300 m scarps on the seafloor, which suggest sub-recent activity. The deeper portions of the accretionary wedge are less well imaged. The decollement can be followed to a maximum depth of 8–9 km (below sea-level), 30–50 km from the E end of the profile. The top basement interface is seen to be gently eastward dipping, parallel to the decollement, but cannot be imaged deeper than about 12 km depth (below sea-level).

SIS-22 crosses the accretionary wedge in a NNW–SSE direction, roughly perpendicular to the to the generally westward tectonic transport direction (Fig. 5). Thus, dipping reflectors and thrust ramps at the N end of the profile (off the Portuguese margin) appear to be N vergent, and conversely, structures at the S end (off the Moroccan margin) appear to be S vergent. In fact, these structures are NW and SW vergent, respectively, along

the lateral ramps of the westward vergent accretionary wedge. Profile SIS-22 images the same major crustal interfaces as profile SIS-16; dipping ramp thrusts soling out to a sub-horizontal decollement, and overlying a basal layer of undeformed sediments above the acoustic basement (Fig. 5). The N and S portions of the profile image the Portuguese and Moroccan continental margins, respectively. Here the basement is known to be continental in nature, and the overlying sediments include carbonate platform strata of Mesozoic age. The basement beneath the accretionary wedge is likely to be a ~150 km corridor of oceanic crust, though the precise nature of this basement and its exact northern and southern limits are unknown. The central portion of the accretionary wedge is >7 km thick (4.5 km of deformed sediments above a 3 km thick basal layer). Top basement here is below 10 km (beneath sea-level), the deepest on this profile.

Time sections of parts of three other MCS profiles are shown which sample the horseshoe-shaped deformation front at different locations and in different orientations (see Fig. 3 for profile locations). Profile SIS-20 samples the western extremity of the deformation front. Here a sharp slope break is present (Fig. 6a). To the west are the undeformed sediments of the Seine Abyssal Plain. The basal series can be followed beneath the accretionary wedge and beneath the decollement. The basal series has a thickness of 2 s TWT, which for a p-wave velocity of 3 km/s represents a thickness of about 3 km. Prominent NE dipping reflectors mark probable ramp thrusts, with one emerging at the seafloor at the slope break. The chaotic facies of the olistostrome are imaged within the Seine Abyssal Plain series, as well as tectonically thickened in the accretionary wedge.

Profile SIS-10 images the chaotic facies of the olistostrome beneath layered sediments in the Seine Abyssal Plain (Fig. 6a). The chaotic facies can be found deformed into an eastward thickening wedge above the decollement. Once again a basal series of subhorizontal undeformed sediments can be seen beneath the decollement. Two dome-shaped features are located at the deformation front and disturb the continuity of reflectors below (Fig. 6c). A similar, although less pronounced feature is seen at the W end of profile SIS-16 (Fig. 4). These may be anticlines related to thrust faulting (fault bend type folds) or diapirs of unknown nature. Only additional observations of the seafloor morphology (bathymetric mapping) can determine whether these are elongated anticlinal ridges or circular diapirs. If circular, they may be mud volcanoes as commonly observed in active accretionary wedges. Alternatively, they may be salt diapirs as observed in SISMAR profiles further SW along the Moroccan margin (Contrucci et al., 2004). If these are salt diapirs, then the underlying basement is probably thinned continental crust and the ocean–continent boundary limit is likely to be located further north (near 35°N). However, without detailed reconnaissance and sampling, this question cannot be resolved.

Profile SIS-14 samples the south-eastern portion of the deformation front. A slope break marks the emergence of a S vergent ramp, thrusting accretionary wedge sediments onto Moroccan margin strata of the Rharb submarine valley. The apparent southward vergence is due to the N–S orientation of the MCS profile across the lateral ramp at the southern boundary of the accretionary wedge (Fig. 3).

3. Depth to basement map

All available multichannel seismic profiles in the study area were used to construct a depth to basement map (Fig. 7). The sub-seafloor sedimentary thickness in two-way way travel time (TWT) was picked at intervals of roughly 10 km. The TWT to the top basement reflection was converted to depth using a mean sedimentary velocity of 3 km/s and these x,y,z points were converted into a grid using the GMT gridding algorithm surface (Wessel and Smith, 1991). On land, depth to basement was taken from published geological maps, which included borehole data in the Guadalquivir and Rharb Basins. Depth to basement was picked directly from the three depth processed MCS lines (SIS-4, SIS-16, and SIS-22). Uncertainties in the depth to basement map may arise from several sources. First, the top basement reflection imaged at the base of a thick sedimentary pile has a low frequency and commonly consists of a triple or quadruple reflection. This 4-part wavelet can reach a thickness of up to 800 m in depth sections and 250 ms TWT in time sections. This can introduce a picking error of ±400 m where the image is unclear. Secondly, the simple 3 km/s p-wave velocity applied for the conversion to depth may be locally inappropriate. Where depth processed and time sections intersect, the results of both techniques can be compared directly. At these crossing points the discrepancy is in all cases ≤500 m. Third, gridding algorithms can introduce local artifacts due to the spline function used. We tested different gridding algorithms with application of low frequency band pass filters. In areas well sampled by seismic reflection profiles, the difference between grids obtained by different methods does not exceed 500 m. Conversely, in outlying regions where no

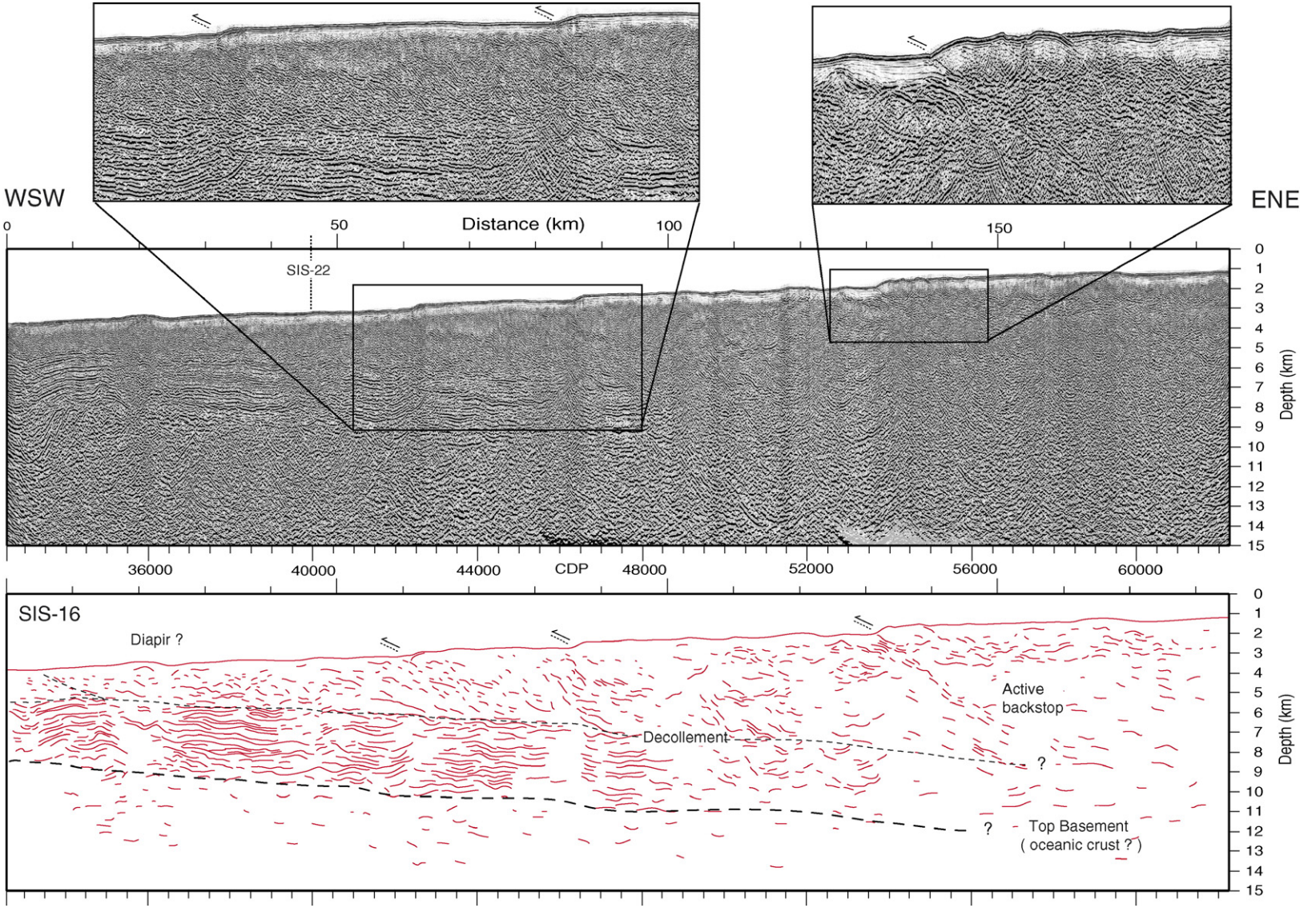

Fig. 4. Multichannel seismic profile SIS-16, pre-stack depth migrated section. Central panel shows the entire 185 km long profile at a vertical exaggeration of 3:1. The lower panel is an interpreted line drawing (a depth cross-section). Upper panels show zooms of ramp thrusts emerging at the seafloor and the basal undeformed strata beneath the decollement. Thin dashed line is the decollement. Thick dashed line is top basement, inferred to be oceanic. Top continental basement has shorter dashing.

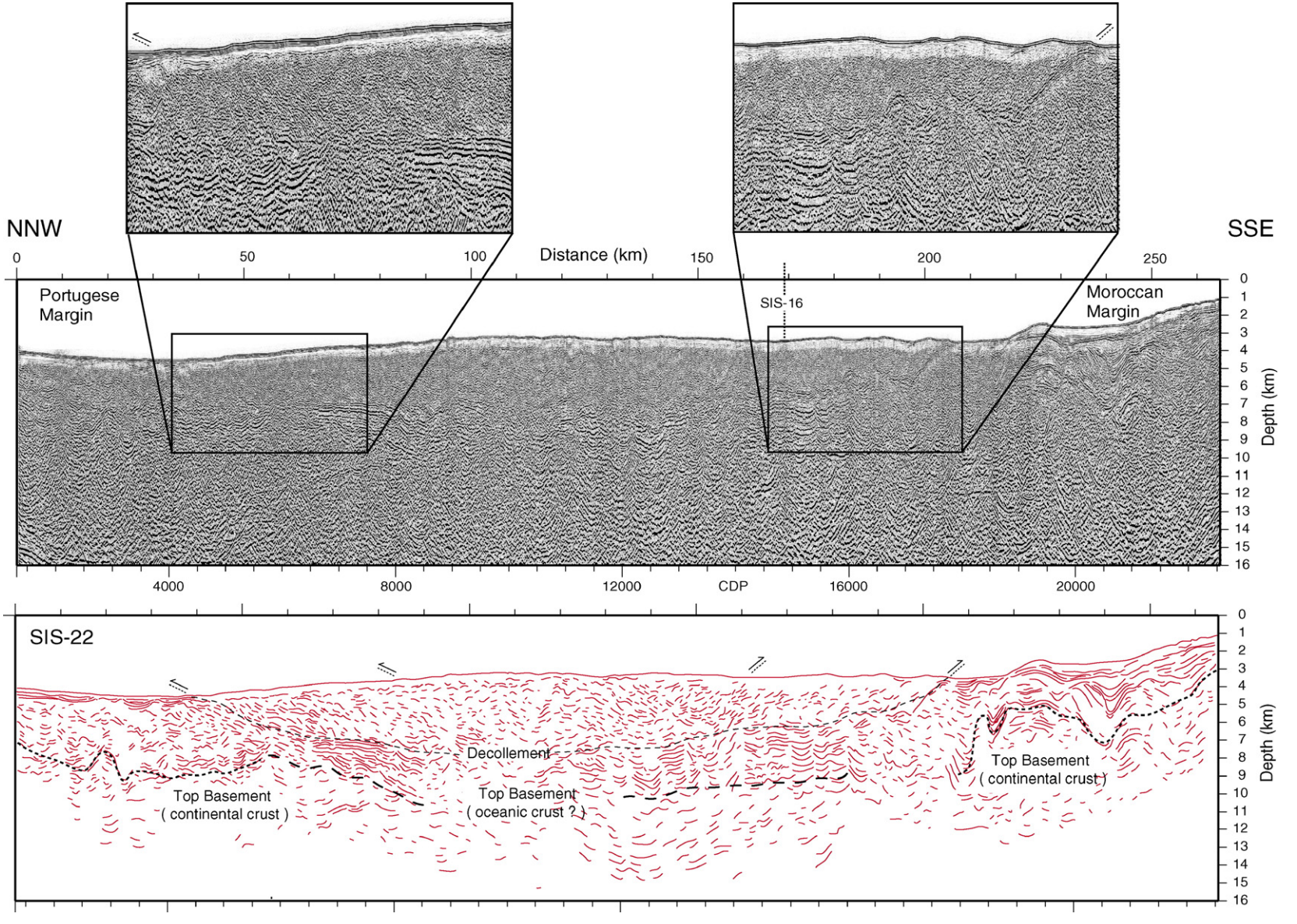

Fig. 5. Multichannel seismic profile SIS-22, pre-stack depth migrated section. Central panel shows the entire 250 km long profile at a vertical exaggeration of 3:1. The lower panel is an interpreted line drawing (a depth cross-section). Upper panels show zooms of ramp thrusts at the deformation front, with the 2 s (TWT) thick basal series below the decollement. (Dashed lines are the same as in Fig. 4.)

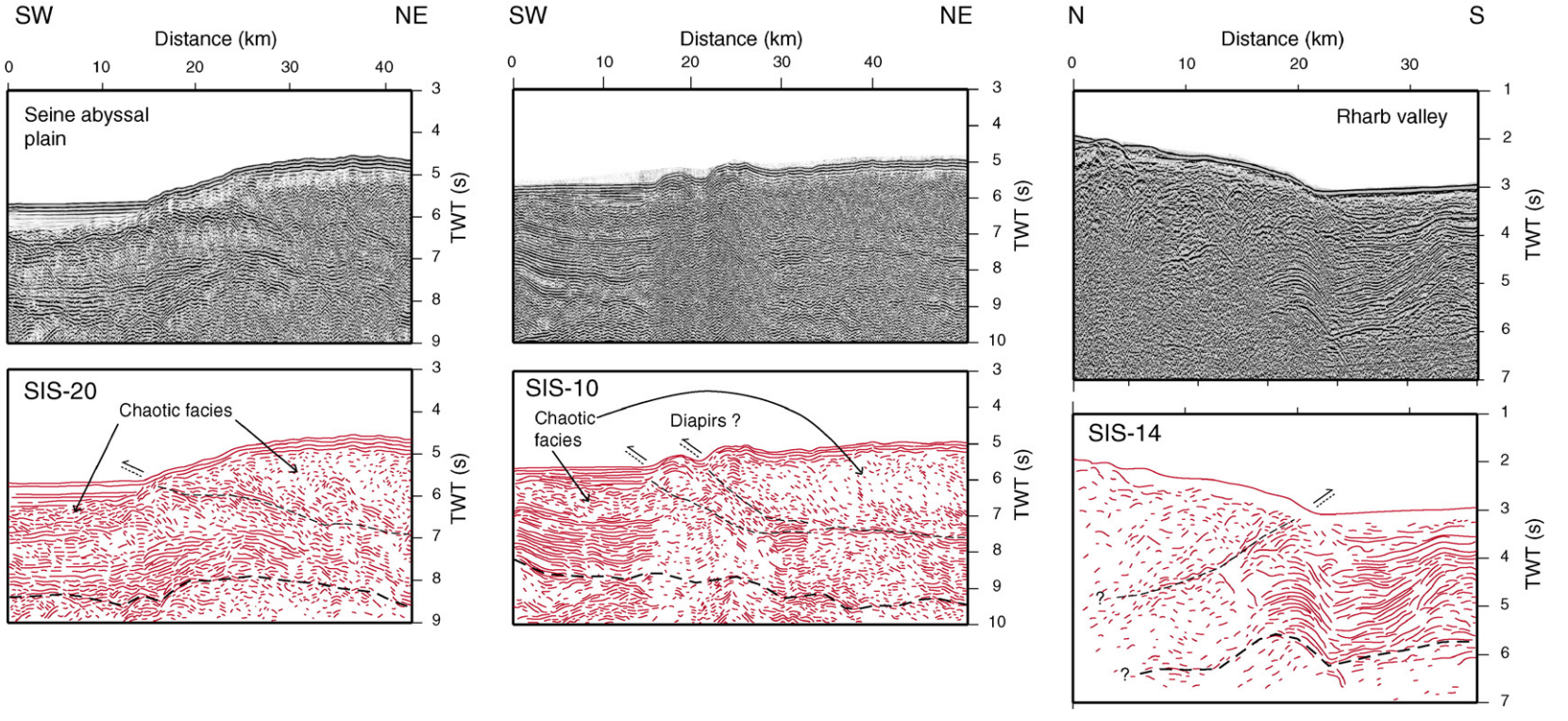

Fig. 6. Close-up views of the deformation front along several SISMAR multichannel seismic profiles accompanied by interpreted line drawings (time sections in TWT). A: SIS-10, B: SIS-14, C: SIS-20. For positions see Fig. 3. (Dashed lines are the same as in Figs. 4 and 5). In each case ramp thrusts can be seen at the deformation front rising to the seafloor from the detachment horizon. A basal series of undeformed horizontal sediments is imaged beneath the decollement. The two dome-shaped features observed on profile SIS-10 may be anticlinal ridges related to ramp thrusts, mud volcanoes or salt diapirs.

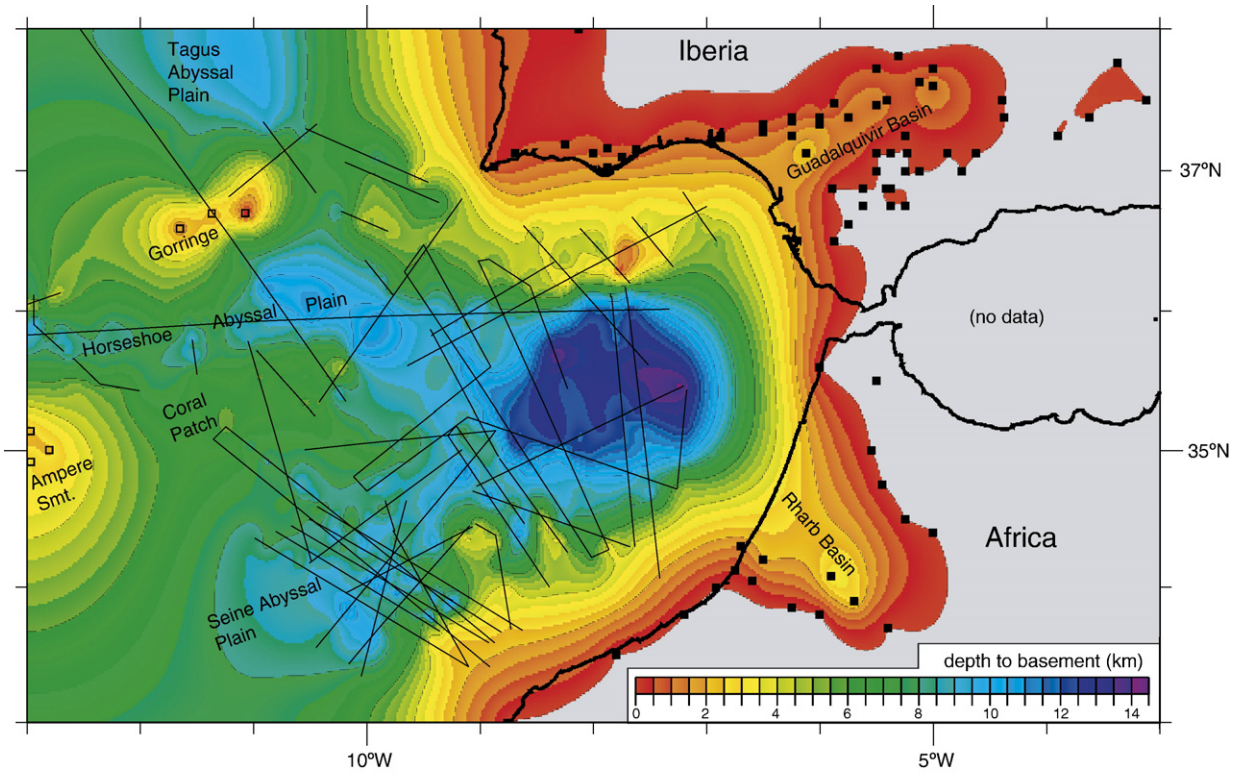

Fig. 7. Depth to basement map obtained by joint interpretation of all SISMAR and other published seismic reflection profiles (Sartori et al., 1994; Tortella et al., 1997; Hayward et al., 1999; Gracia et al., 2003a,b; Zitellini et al., 2004) from the study area. Sub-seafloor sedimentary thicknesses in two-way travel time (TWT) were converted to depth using a mean p-wave velocity of 3 km/s. Land picks (black squares) are based on the limit of outcropping basement and borehole data, as indicated on the geological map (International Geological Congress, 1968). Some picks at sea (open squares on Gorringe and Ampere) are based on basement outcrops reported here (Hayward et al., 1999).

seismic data are available, the depth to basement remains unconstrained and local basement highs or sub-basins may exist.

The final depth to basement map obtained shows a general E–W oriented trough in the Gulf of Cadiz. On the SW Iberian margin and the NW Moroccan margin, depth to basement is typically <5 km and decreases to 0.5–2 km near the coastline. Below the adjacent abyssal plains, the mean depth to basement is around 9 km. Within the E–W trough, there is a gradual eastward increase in depth to basement, reaching maximum values of 12–13 km. The decollement, as imaged on the MCS profiles discussed above, is located about 3 km above the basement, above a basal unit of undeformed layered sediments. Thus, although the depth to basement map is not an exact measure of the depth to the fault plane, the geometry of the two interfaces is directly related. The region of greatest basement depth terminates to the east in a crescent-shaped trough, sub-parallel to the Betic–Rif mountain belt.

4. Gravity constraints on the subduction fault plane

Deep seismic profiles can seldom image structures below 10–15 km depth. Gravity modeling can be used to help constrain the crustal structure at such depths where the seismic energy may not penetrate. The free-air gravity map of the region shows an overall similarity to the depth to basement map, with a triangular minimum in the Gulf of Cadiz reaching values of −100 mGal (Fig. 8a). A 2-D gravity model was constructed along section A–A′ profile (crossing the accretionary wedge, the Betic–Rif orogen and extending into the western Mediterranean domain of the Alboran Sea). Where available, the known shallow crustal structure (from seismic profiles) was integrated into the model. Crustal structure in the Alboran Sea was taken largely from an earlier synthesis showing thinned continental crust (10–15 km thick) overlain by 4–7 km thick sediments across most of the West Alboran Sea (Docherty and Banda, 1995). The continental nature of the crust was confirmed by ODP drilling on a basement high during Leg 161 at

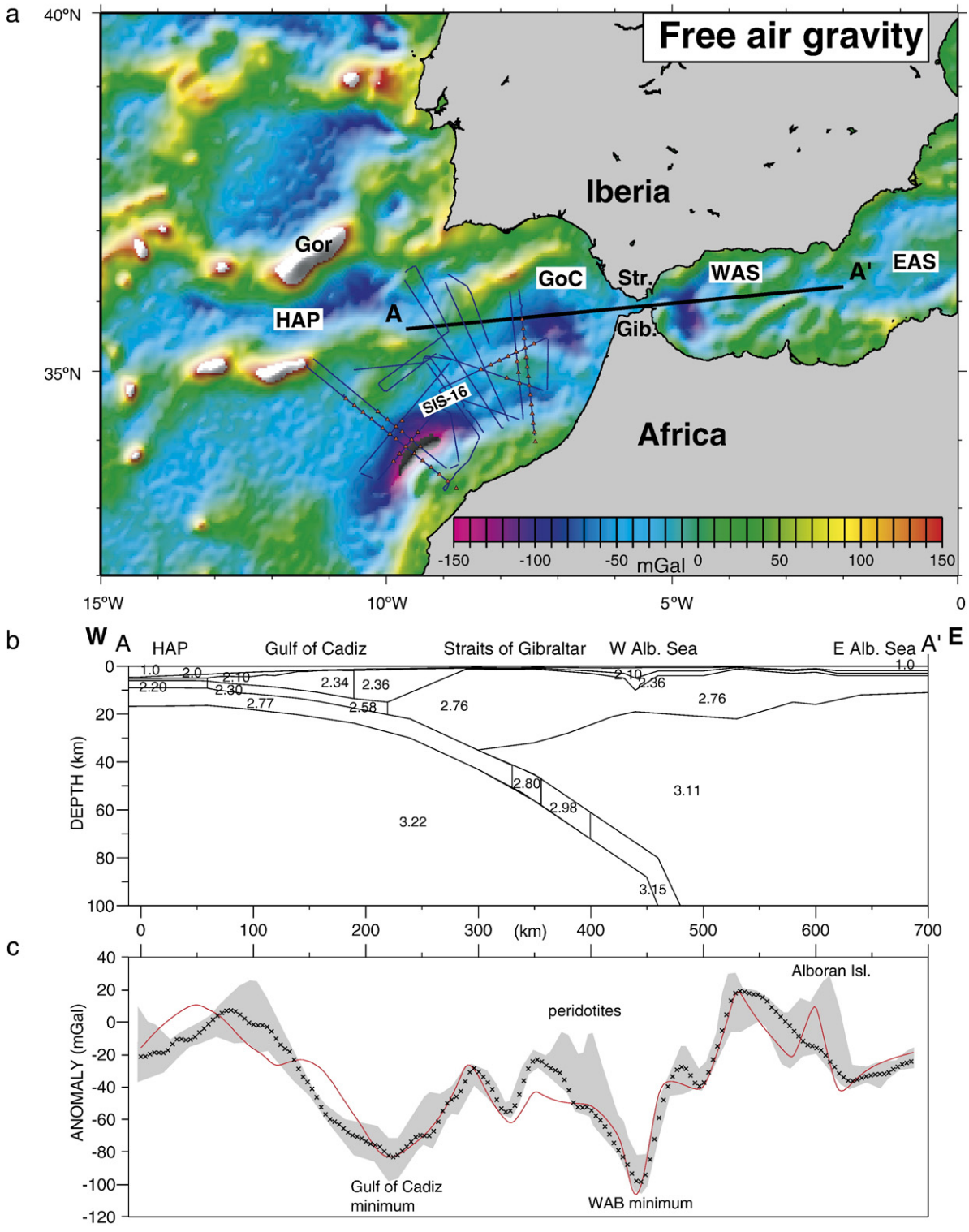

Fig. 8. Free-air gravity of the study area (a) Free-air gravity map (Sandwell and Smith, 1997), (b) density model, (c) calculated (red line) and observed (black crosses) free-air gravity anomaly along section A–A′. The gray shaded region indicates the maximum and minimum anomaly observed within a band 10 km N and 10 km S of profile A–A′ in order to illustrate local 3-D effects due to small scale variations in upper crustal structure. Gor=Gorringe Bank, HAP=Horseshoe Abyssal Plain, GoC=Gulf of Cadiz, Str. Gib.=Straits of Gibraltar, WAS=West Alboran Sea, EAS=East Alboran Sea.

site 974 (Comas et al., 1999). Recently acquired, but unreleased industry data indicate 12 km of continuous sedimentary strata in the crescent-shaped West Alboran basin (Kuo et al., 2002; Weinzapfel et al., 2003). These crustal and sedimentary thicknesses were used as a starting point for constructing the density model (Fig. 8b,c).

The free-air gravity signal along a 700 km E–W profile has a roughly "W" shape, with two minima of −90 to −100 mGal, beneath the eastern Gulf of Cadiz and the western West Alboran Sea, respectively. The 80–90 mGal drop from the Horseshoe Abyssal Plain to the eastern Gulf of Cadiz is well modeled by an eastward thickening wedge of fairly low-density sediments. The density structure in the accretionary wedge region is based on the published OBS velocity model (Gutscher et al., 2002). A maximum thickness of 15 km of accretionary wedge sediments, overlying another 5 km basal layer is modeled near the gravity minimum. This compares to a maximum of 10 km and 4 km, respectively, as inferred at the E termination of seismic profile SIS-16 (which corresponds to a position approximately 50 km further west). A slight misfit near km 100 is probably due to 3-D effects of an oblique basement ridge crossing the front of the profile.

The density of the subducting oceanic crust increases with depth below 40 km from 2.77 g/cm^3 to 3.15 g/cm^3, to account for the basalt to eclogite mineralogical transformation. The upper mantle density beneath the Alboran Sea (3.11 g/cm^3) is lower than beneath the Gulf of Cadiz (3.22 g/cm^3), in accordance with the different thermal state of the two domains. The Alboran Sea has warm, convecting back-arc upper mantle (with arc volcanism until 5 Ma), active crustal extension, and is marked by a low p-wave velocity anomaly. The Gulf of Cadiz domain is underlain by cold, 130 Ma oceanic upper mantle and marked by a high p-wave velocity anomaly (Gutscher et al., 2002).

The local gravity maxima (absolute value of −20 mGal) in the Straits of Gibraltar are associated with metamorphic rocks in the core of the Betic–Rif mountain belt and an absence of low-density Neogene sediments. A misfit is present at km 350 (and up to km 400 along a 20 km wide parallel band–see gray shading in Fig. 8c), where the calculated signal is about 20 mGal lower than the observed free-air gravity. This corresponds to the structural position of the Ronda and Beni–Bousera peridotite massifs, exhumed slivers of upper mantle rocks, exposed along the innermost arc of the Betic–Rif belt. Another very deep crescent-shaped minimum (−100 mGal) is situated in the West Alboran Sea and correlates with the West Alboran Basin (WAB), with sedimentary thicknesses, ranging from 5–7 km to the north, near the Spanish coast (Docherty and Banda, 1995; Comas et al., 1999) to 12 km at the gravity minimum (Kuo et al., 2002; Weinzapfel et al., 2003). Gravity maxima of about +10 mGal are associated with basement highs near Alboran Island. As the profile enters the Eastern Alboran Sea, the gravity signature shows little variation, remaining at about −20 mGal. The basement here may be oceanic in nature (Docherty and Banda, 1995; Comas et al., 1999).

5. Thermal modeling of the Gibraltar arc and seismogenic zone

We apply steady-state, finite-element modeling of forearc thermal structure in order to test the active subduction hypothesis and to determine the updip and downdip limits of the seismogenic zone. Numerical modeling of forearc thermal structure is commonly used to determine the temperature distribution along the subduction zone thrust. Stick–slip rheological behavior leading to earthquake rupture, is widely considered to be controlled by temperature (Hyndman et al., 1995; Peacock and Wang, 1999; Gutscher and Peacock, 2003). The geometry of the subduction interface in two dimensions is constrained by several different types of data. Depth sections from seismic reflection profiles (e.g. Fig. 4) and OBS profiles (Gutscher et al., 2002) image the crustal structure of the frontal 150 km down to a maximum depth of 15 km. The distribution of hypocenters helps constrain the central portion between 20 and 100 km depth (Fig. 9) and tomographic images reveal the deep geometry between 100 and 660 km depth (Gutscher et al., 2002) (Fig. 9, inset). These data have been combined to construct the 2-D finite-element grid, which reflects the strong curvature of the steepening slab (Fig. 9).

We used finite-element (FE) software developed by Kelin Wang and co-workers (Hyndman et al., 1995; Peacock and Wang, 1999). The 700 km long FE-model consists of 1296 quadrilateral elements, with 4033 nodes. The model includes the effects of radiogenic heating in the crust, shear heating along the subduction interface with an effective shear stress of 10 MPa, and viscous corner flow in the mantle wedge. (Values for radiogenic heating and thermal conductivities in the continental and oceanic crust, respectively, are given in Peacock and Wang, 1999.) Low p-wave velocities observed in tomographic cross-sections indicate the presence of hot convecting asthenosphere at shallow depth (40–80 km depth) beneath West Alboran Sea and the Straits of Gibraltar (Gutscher et al., 2002) and thus a

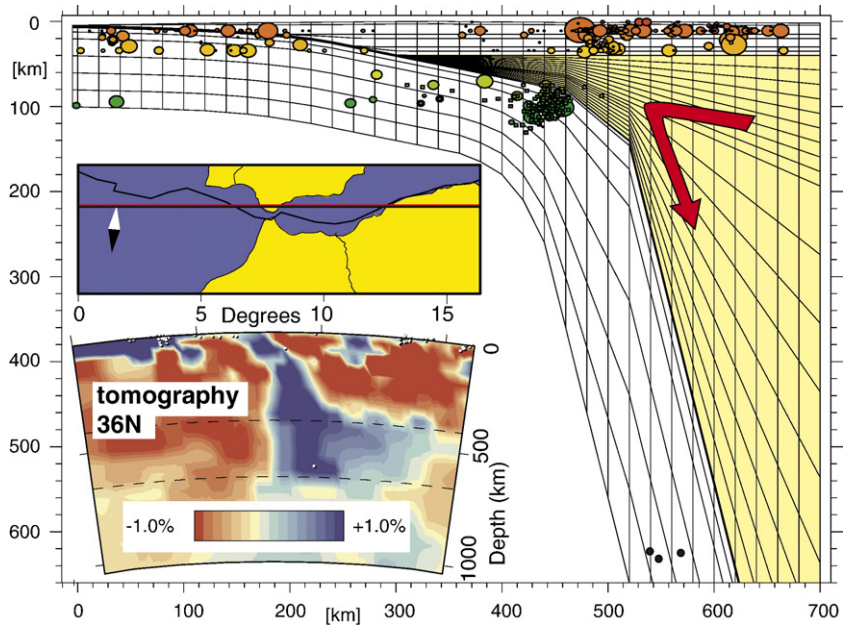

Fig. 9. Finite-element grid used for calculating the thermal structure of the Gibraltar arc along profile A–A′ (for location of profile see Figs. 1 and 8). Boundary conditions include; GDH1 thermal structure for 130 Ma old oceanic lithosphere at the left side (Stein and Stein, 1992), and a 40 km thick upper plate with a hot thermal structure equivalent to 10 Ma old oceanic lithosphere at the right side. Inset shows tomographic image along an E–W cross-section at 36°N latitude (Gutscher et al., 2002) used to constrain the deep geometry (from 50 to 660 km depth). Note the presence of a wedge of low velocity material (light, hot asthenosphere) beneath the West Alboran Sea and the Straits of Gibraltar.

composite mantle wedge with slab dips of 14°, 45° and 79° was used to represent this complex geometry. The initial boundary conditions include: at the left side, oceanic lithosphere isotherms for the subducting plate of the appropriate age based on the GDH1 thermal cooling model (Stein and Stein, 1992), 0° C at the surface and an appropriate continental or oceanic geotherm at the right side boundary (representing the upper plate). The three primary input parameters to the model are thus; the plate geometry, the age of the subducting lithosphere and the subduction velocity.

The exact age of the subducting oceanic lithosphere is not known. Plate kinematic reconstructions of the opening of the western Tethys between Africa and Eurasia suggest that it post dates Triassic–Jurassic rifting in the Central Atlantic (Stampfli et al., 2001). Radiometric dating of zircons in the Ronda and Beni–Bousera peridotites in the Betic and Rif mountain belts indicate the age of rifting in the sub-continental mantle to be 180–130 Ma (Sanchez-Rodriguez and Gebauer, 2000). Our model includes a 130 Ma old subducting plate, although an age of 180 Ma would not significantly alter the thermal structure, since most cooling occurs in the first 50–100 m.y. (Stein and Stein, 1992). The upper plate in the westernmost Alboran Sea is known from ODP Leg 161 drilling to consist of thinned continental crust, though further east in the East Alboran Sea, the basement may be oceanic in nature (Comas et al., 1999).

The kinematics of this small subduction system is driven by the gravitational force of the sinking slab of oceanic lithosphere and subsequent slab rollback to the west. As a result, the subduction velocity is not directly related to the large-scale plate motion between Africa and Eurasia. The convergence rate, relevant for thermal modeling and for earthquake occurrence, is the relative motion of the slab in the reference frame of the overriding plate (in this case, the Gibraltar block). A simple reconstruction of the position of the paleo-volcanic arc (Duggen et al., 2003) with respect to the current position of the 100 km depth contour to the slab, suggests approximately 200 km of westward movement of the Gibraltar block since 10 Ma, and thus a mean velocity of 20 mm/a (Gutscher et al., 2002). Available GPS data from 3 years of observation in NW Morocco and Southern Iberia indicate stations in the Gibraltar block moving with a velocity of 5–10 mm/a in a WSW direction (with respect to Eurasia), independent of the 4 mm/a NW motion of African plate stations in NW Morocco (Reilinger et al., 2001; Mourabit et al., 2002). Thus, subduction velocities between 1 and 20 mm/a were tested (Fig. 10).

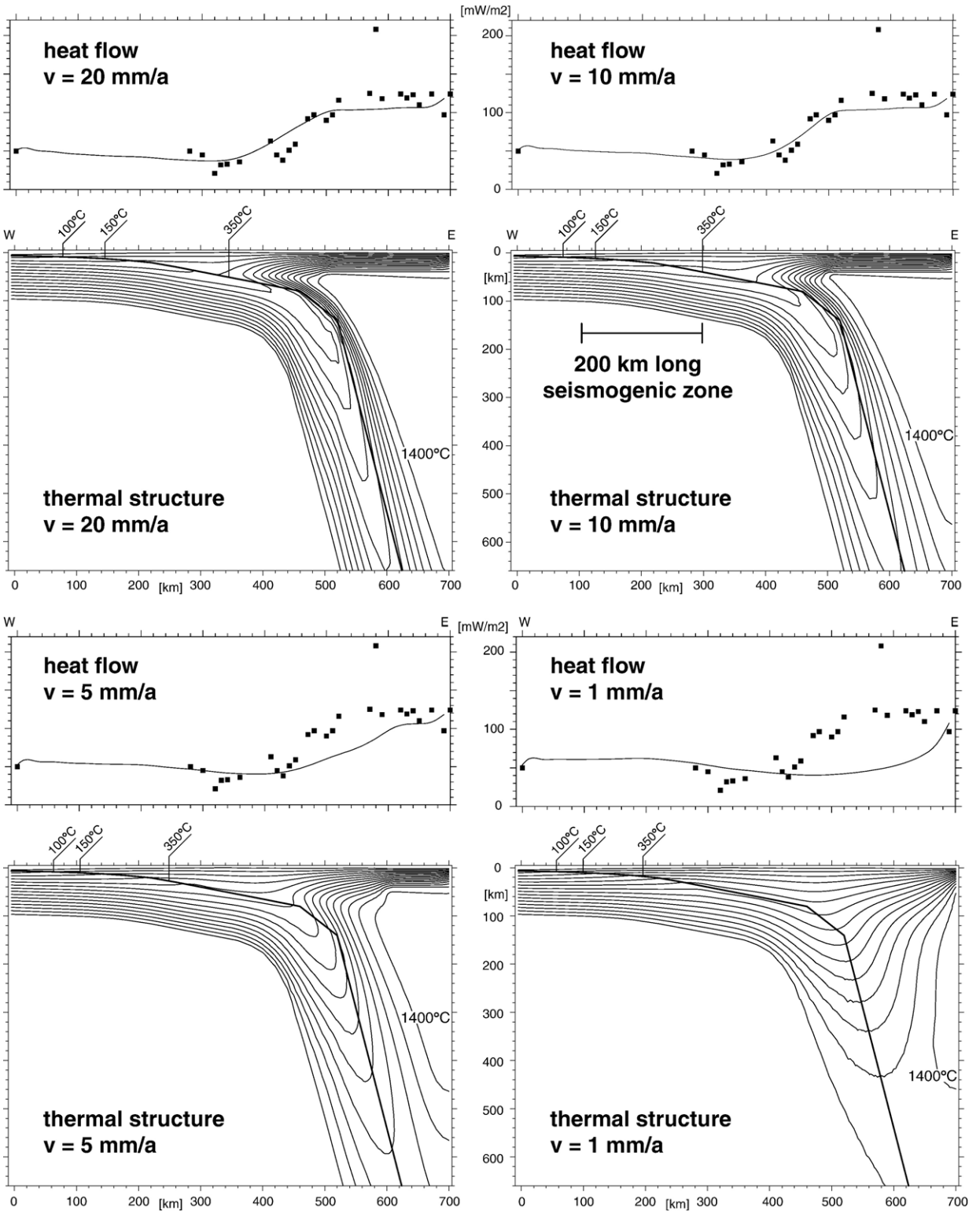

Fig. 10. Thermal models of Gibraltar arc along profile A–A′ for different velocities of the subducting slab (with respect to the overriding Gibraltar block). In each case the resulting steady-state thermal structure is shown with the calculated and observed heat flow above (100 °C isocontours with 0 °C at surface and 1400 °C in asthenospheric mantle). The best fit to observed heat flow data and to the distribution of hot material seen in tomography (Fig. 9, inset) is obtained for a subduction velocity of 10 mm/a, which predicts a 200 km downdip width of the seismogenic zone.

Heat flow data are available from land data in Iberia as well as abundant in situ marine measurements in the Alboran Sea (Fernandez et al., 1998; Torne et al., 2000). Some data are available as well for the Rif chain of northern Morocco (Rimi et al., 1998). Available data within 50 km of section A–A′ were compiled and used to compare to the numerically calculated heat flow (Fig. 10). Only one measured heat flow value is available for the Gulf of Cadiz or the abyssal plains located to the west and indicates low heat flow (50 mW/m^2). Heat flow is even lower in the vicinity of the Straits of Gibraltar, with values in the nearby Betic and Rif from 20 to 40 mW/m^2. Heat flow increases to 60–100 mW/m^2 in the Western Alboran Sea before reaching a nearly constant value of 100–120 mW/m^2 in the Central and Eastern Alboran Sea. The high heat flow in the upper plate in the Alboran domain is equivalent to that of 10 m.y. old oceanic lithosphere, but the upper plate is known to be highly thinned continental crust, as drilled in ODP Site 974 (Comas et al., 1999). The easternmost 50–100 km of the profile may indeed be oceanic crust of uncertain (Oligo-Miocene age).

Four modeled temperature distributions are shown for subduction velocities of 1–20 mm/a (Fig. 10). The best fit to observed heat flow data and to the distribution of hot material seen in tomography (Fig. 9, inset) is obtained for a subduction velocity of 10 mm/a and indicates vigorous convection in the upper mantle. Lower subduction velocities do not result in sufficiently high heat flow in the back-arc region of the Alboran Sea. Nor can such slow velocities (5–1 mm/a) explain the rapid transfer of cold lithosphere to the 660 km discontinuity, as required by deep focus seismicity. Furthermore, very slow to inactive subduction cannot generate the wedge-shaped zone of hot material seen in the tomographic sections beneath the West Alboran Sea and Straits of Gibraltar. However, the steady-state thermal modeling applied here does not take into account any hypothetical very recent changes in the subduction parameters (like subduction velocity for instance). The thermal relaxation time of the lithosphere being several million years, the subduction velocity of 10 mm/a should thus be considered an average rate over time. The current velocity may have slowed significantly.

Regarding the interplate seismogenic zone, the updip limit is considered to be represented by the 100–150 °C isotherms and the 350 °C isotherm is considered to mark the downdip limit of the seismogenic zone (Hyndman et al., 1995). For the 10 mm/a thermal model, these temperatures are reached 80–120 km from the deformation front and 300 km from the deformation front, respectively. This corresponds to a downdip width of 200 km for the seismogenic zone (Fig. 10).

6. Discussion

In order to address the hypothesis that a subduction earthquake produced the Lisbon earthquake it must be shown that the fault area is sufficiently large and potentially active. The 3-D geometry of the fault surface as constrained by existing seismic data is presented above. Together with the updip and downdip limits indicated by the thermal modeling, the potential locked zone is shown to have dimensions of about 180×200 km^2. For uniform co-seismic slip values of 10–20 m, moment magnitudes of Mw 8.6–8.8, respectively, are obtained (Gutscher et al., 2006-this volume). These calculated magnitudes are consistent with the wide felt area and the great intensities recorded during the 1755 earthquake (Martinez-Solares et al., 1979; Johnston, 1996). The fault dimensions and seismic moment are also in fairly good agreement with empirical rupture length–moment relationships determined from statistical studies of other earthquakes (Wells and Coppersmith, 1994; Gutscher et al., 2006-this volume).

Concerning the activity of the Gibraltar subduction system, the two most obvious indicators of active subduction are lacking; an active volcanic arc and shallow thrust type earthquakes. These two points will be discussed first and then other indirect evidence of active subduction will be presented.

Geochemical studies of magmatic rocks in the West Alboran Sea were performed and demonstrate unequivocally the existence of a subduction related volcanic arc between 15 and 5 Ma with major and trace element signatures similar to the Izu–Bonin and Aeolian arcs (Duggen et al., 2003, 2004). Volcanism became increasingly K-rich before calc–alkaline (subduction related) volcanism ceased around 4.8 Ma. This shift in geochemistry is similar to that observed in the Aeolian/Calabrian arc (Duggen et al., 2004). This suggests that as the width of the subducting oceanic domain narrows, calc–alkaline volcanism may cease due to changes in the style of convection in the back-arc mantle. Oligo-Miocene subduction volcanism effectively refutes the commonly evoked delamination model for the evolution of the Alboran Sea (Platt and Houseman, 2003; Gutscher et al., 2003). Although a complete discussion of delamination models (peeling off of overthickened orogenic lithosphere) is beyond the scope of this paper, we note that while active/recent delamination may offer similar thermal characteristics (to active subduction thermal models), it cannot explain continued W vergent

thrusting in the Gulf of Cadiz, with simultaneous subsidence in the West Alboran Sea. Furthermore, active delamination (if postulated) would predict a belt of ultra-rapid uplift above the delamination hinge line, a prediction not supported by observations of modest uplift (0.1 mm/a) reported for the Gibraltar block (Zazo et al., 1999).

No instrumentally recorded subduction interface earthquakes (events with a shallow east dipping, thrust-type focal mechanism) are known in the Gulf of Cadiz. Therefore, either subduction here has ceased (no seismogenic zone), subduction is active and aseismic, or subduction is active and the seismogenic zone is currently locked. We favor the latter interpretation, in which case the Gibraltar subduction zone would exhibit a similar behavior as the Nankai or Cascadia subduction zones, which are characterized by a large locked zone, and a recurrence time of 100–1000 years for great earthquakes (Satake, 1993; Hyndman et al., 1995; Clague, 1997). In general, Cascadia and Nankai are moderately slow (3–5 cm/a) subduction zones with thick trench fill (1.5–3 km). The Gibraltar–Cadiz system, with a velocity of ≤1 cm/a and 5 km of sedimentary input, may be an extreme end-member of the slow and thickly sedimented convergent margin type.

The earthquake hypocenters shown in map view and cross-sections (Figs. 1, 2 and 9) are from the USGS/NEIC PDE Catalog (1973–2003), with a location uncertainty typically of ±10 km. The intermediate depth seismicity in the West Alboran Sea and the deep focus seismicity beneath Granada (Southern Spain) are well documented by numerous detailed studies (Buforn et al., 1991; Casado et al., 2001). The distribution of intermediate and deep focus seismicity within the east dipping high p-wave velocity slab imaged by tomographic data (Fig. 9, inset) is entirely consistent with east dipping subduction (Gutscher et al., 2002) and difficult to explain otherwise. Finally, seismological studies of deep focus events recorded by local stations indicate continuity of high Q material (dense, cold slab) from >600 km depth to the surface (Okal, 2001).

The Gibraltar arc system exhibits other geophysical features characteristic of trench–arc systems around the world. Heat flow data reflect the typical pattern of a forearc thermal low (35 mW/m^2) and back-arc thermal high (>100 mW/m^2) (Stein, 2003). The free-air gravity follows the classic low-high pattern, with a −100 mGal minimum near the "trench" centered over the thick wedge of deformed sediments, and a relative maximum (−30 mGal) in the forearc block.

Numerous studies relevant to the question of active subduction have been completed in the past few years and more are planned in the near future. Active mud volcanoes have been identified across vast portions of the Gibraltar accretionary prism and down to 3500 m water depth (Pinheiro et al., 2003). Mud volcanoes are commonly observed in accretionary wedges (Barbados Ridge, Mediterranean Ridge) and caused by dewatering and excess fluid pressure in actively deforming, young, high porosity sediments (Kopf et al., 2001).

Active E–W extension in the West Alboran Sea is suggested by three types of data; earthquake focal mechanisms, seismic profiles and GPS data. Earthquake focal mechanisms for shallow (<30 km depth) crustal earthquakes in the West Alboran Sea show predominantly normal faulting mechanisms with N70°E oriented T axes indicating E–W extension (Stich et al., 2003). Multichannel seismic profiles across the West Alboran Basin show a 1–1.5 s TWT sediment layer above the Messinian unconformity (Watts et al., 1993). This represents 1–1.5 km of Plio-Quaternary sediments (for a mean p-wave velocity of 2 km/s) and suggests an equivalent amount of subsidence, likely related to crustal extension. Finally, GPS data show differential WSW motion of stations in the Rif at 5–10 mm/a, with respect to stable Eurasia (Madrid fixed reference frame) and with respect to stations in NE Morocco (Reilinger et al., 2001; Mourabit et al., 2002). This has been interpreted as evidence for active ENE–WSW extension in the West Alboran Sea (Mourabit et al., 2002). Active E–W extension in the back-arc is mechanically incompatible with delamination models and perhaps offers the ultimate test of the active subduction and slab rollback model. Establishing the timing and quantity of extension in the West Alboran Sea will require future studies.

7. Conclusions

Evidence for active subduction is presented here, in the form of seismic images of ramp faults cutting to the seafloor at the base of steep morphologic scarps. Seismic profiles image the deformation front at numerous locations arrayed along a horseshoe pattern in the deep Gulf of Cadiz at 2000–4300 m water depth (Fig. 3). The same pattern is observed repeatedly; undeformed horizontal basal reflectors, beneath a detachment horizon, seaward vergent (W, SW or NW) ramps intersecting the seafloor at a slope break between the horizontal abyssal plain surface, and the gentle 1° undulating surface slope at the toe of the accretionary wedge (Figs. 4–6). The east dipping decollement and

top basement interfaces demonstrate that deformation is tectonic and not gravitational in origin.

The heat flow models presented offer further proof of active subduction (Fig. 10). Only an actively sinking slab can generate the vigorous back-arc convection and rapid transfer of cold lithosphere to the 660 km discontinuity. These characteristics (offered by models with subduction velocities of 10–20 mm/a) are necessary to explain the high back-arc heat flow (120 mW/m^2 in the West Alboran Sea) as well as deep focus seismicity at 660 km depth. Very slow to inactive subduction cannot generate the wedge-shaped zone of hot material seen in tomographic sections. Thermal modeling indicates a 200 km downdip width of the seismogenic zone. Together with the seismic data, a potentially locked subduction fault plane with dimensions of about 180 km (N–S)×200 km (E–W) is indicated. Such a fault is capable of generating an M=8.6–8.8 earthquake for 10–20 m of co-seismic slip.

Future marine geophysical surveys will be conducted in the Gulf of Cadiz in order to perform bathymetric swath mapping of the accretionary prism and the adjacent regions, to collect heat flow data in a region with almost no data coverage and to identify and sample mud volcanoes and other diapiric structures near the deformation front. With the benefit of these additional data it should be possible to determine conclusively whether active west vergent deformation is occurring presently in the Gulf of Cadiz.

Acknowledgments

We thank Dirk Klaeschen for assistance during pre-stack depth processing at GEOMAR Processing Centre and the European Community for its support granted to this Large Scale Facility. We also thank Roy Hyndman, an anonymous reviewer and Editor Pierre Henry for constructive suggestions, which helped to improve the original manuscript. E.T.'s PhD research was supported by a stipend from the French Ministry of Education and Research. This article is IUEM contribution 992.

References

Argus, D.F., Gordon, R.G., Demets, C., Stein, S., 1989. Closure of the Africa–Eurasia–North America plate motion circuit and tectonics of the Gloria fault. J. Geophys. Res. 94, 5585–5602.

Baptista, M.A., Heitor, S., Miranda, J.M., Miranda, P.M.A., Mendes Victor, L., 1998. The 1755 Lisbon; evaluation of the tsunami parameters. J. Geodynamics 25, 143–157.

Buforn, E., Udias, A., Madariaga, R., 1991. Intermediate and deep earthquakes in Spain. Pure Appl. Geophys. 136, 375–393.

Byrne, D.E., Davis, D.M., Sykes, L.R., 1988. Loci and maximum size of thrust earthquakes and the mechanics of the shallow region of subduction zones. Tectonics 7, 833–857.

Casado, C., Sanz de Galdeano, C., Palacios, S., Romero, J., 2001. The structure of the Alboran Sea: an interpretation from seismological and geological data. Tectonophysics 338, 79–95.

Clague, J.J., 1997. Evidence for large earthquakes at the Cascadia subduction zone. Rev. Geophys. 35, 439–460.

Comas, M.C., Platt, J.P., Soto, J.I., Watts, A.B., 1999. The origin and tectonic history of the Alboran Basin: insights from Leg 161 results. Proc. Ocean Drill. Program: College Station, Texas, vol. 161, pp. 555–579.

Contrucci, I., Klingelhoefer, F., Perrot, J., Bartolome, R., Gutscher, M.-A., Sahabi, M., Malod, J., Rehault, J.-P., 2004. The crustal structure of the NW-Moroccan continental margin from wide-angle and reflection seismic data. Geophys. J. Int. 158, 529–553.

Docherty, C., Banda, E., 1995. Evidence for the eastward migration of the Alboran Sea based on regional subsidence analysis: a case for basin formation by delamination of the subcrustal lithosphere? Tectonics 14, 804–818.

Duggen, S., Hoernle, K., van den Bogaard, P., Ruepke, L., Phipps-Morgan, J., 2003. Deep roots of the Messinian Salinity Crisis. Nature 422, 602–606.

Duggen, S., Hoernle, K., van den Bogaard, P., Harris, C., 2004. Magmatic evolution of the Alboran Region: the role of subduction in forming the western Mediterranean and causing the Messinian Salinity Crisis. Earth Planet. Sci. Lett. 218, 91–108.

Faccenna, C., Becker, T.W., Pio Lucente, F., Jolivet, L., Rosetti, F., 2001. History of subduction and back-arc extension in the Central Mediterranean. Geophys. J. Int. 145, 809–820.

Fernandez, M., Marzan, I., Correia, A., Mezcua, J., 1998. Heat flow, heat production, and lithospheric thermal regime in the Iberian Peninsula. Tectonophysics 291, 29–53.

Flueh, E.R., Fisher, M.A., Bialas, J., Childs, J.R., Klaeschen, D., Kukowski, N., Parsons, T., Scholl, D.W., ten Brink, U., Tréhu, A.M., Vidal, N., 1998. New seismic images of the Cascadia subduction zone from Cruise SO108–ORWELL. Tectonophysics 293, 69–84.

Gracia, E., Danobeitia, J.J., Verges, J., PARCIFAL TEam, 2003a. Mapping active faults offshore Portugal (36°N–38°N): implications for seismic hazard assessment along the southwest Iberian margin. Geology 31, 83–86.

Gracia, E., Danobeitia, J.J., Verges, J., Bartolome, R., 2003b. Crustal architecture and tectonic evolution of the Gulf of Cadiz (SW Iberian margin) at the convergence of the Eurasian and African plates. Tectonics 22 (4), 1033. doi:10.1029/2001TC901045.

Gutscher, M.-A., 2004. What caused the Great Lisbon earthquake? Science 305, 1247–1248.

Gutscher, M.-A., Peacock, S.M., 2003. Thermal models of flat subduction and the rupture zone of great subduction earthquakes. Journal of Geophysical Research 108, 2009.

Gutscher, M.-A., Malod, J., Rehault, J.-P., Contrucci, I., Klingelhoefer, F., Mendes-Victor, L., Spakman, W., 2002. Evidence for active subduction beneath Gibraltar. Geology 30, 1071–1074.

Gutscher, M.-A., Malod, J., Rehault, J.-P., Contrucci, I., Klingelhoefer, F., Mendes-Victor, L., and Spakman, W., 2003. Reply to Comment by John Platt and Greg Houseman on: Evidence for active subduction beneath Gibraltar, Geology, v. 31, n.6, p. e23. (Online Forum http://www.gsajournals.org/gsaonline/?request=get-static&name=i0091-7613-31-6).

Gutscher, M.-A., Baptista, M.A., Miranda, J.M., 2006. The Gibraltar Arc seismogenic zone: Part 2. Constraints on a shallow east

dipping fault plane source for the 1755 Lisbon earthquake provided by tsunami modeling and seismic intensity. Tectonophysics 426, 153–166 (this volume).

Hayward, N., Watts, A.B., Westbrook, G.K., Collier, J.S., 1999. A seismic reflection and GLORIA study of compressional deformation in the Gorringe Bank region, eastern North Atlantic. Geophys. J. Int. 138, 831–850.

Hyndman, R.D., 1995. Thermal constraints on the seismogenic portion of the southwestern Japan subduction thrust. J. Geophys. Res. 100, 15373–15392.

IOC, IHO, BODC, 2003. "Centenary edition of the GEBCO Digital Atlas", published on CD-ROM on behalf of the Intergovernmental Oceanographic Commission and the International Hydrographic Organization as part of the General Bathymetric Chart of the Oceans; British Oceanographic Data Centre, Liverpool.

International Geological Congress, 1968. International Tectonic Map of Africa. eds. G. Choubert, A. Faure-Muret and J. Sugy, UNESCO Commission for the World Geological Map, Subcommission for the World Tectonic Map.

Jimenez-Munt, I., Fernandez, M., Torne, M., Bird, P., 2001. The transition from linear to diffuse plate boundary in the Azores–Gibraltar region. Earth Planet. Sci. Lett. 192, 175–189.

Johnston, A., 1996. Seismic moment assessment of earthquakes in stable continental regions: III. New Madrid, 1811–1812, Charleston 1886 and Lisbon 1755. Geophys. J. Int. 126, 314–344.

Kopf, A., Klaeschen, D., Mascle, J., 2001. Extreme efficiency of mud volcanism in dewatering accretionary prisms. Earth Planet. Sci. Lett. 189, 295–313.

Kuo, L.C., Mountfield, R.A., Chevalier, Y.M., Haddad, A.C., Weinzapfel, A.C., Strickland, M.O., 2002. Petroleum system and exploration potential of the West Alboran Basin. Proc. of Am. Assoc. Petr. Geologists Meeting, Cairo, 2002 (abstract).

Lonergan, L., White, N., 1997. Origin of the Betic–Rif mountain belt. Tectonics 16, 504–522.

Martinez-Solares, J.M., Lopez, A., Mezcua, J., 1979. Isoseismal map of the 1755 Lisbon earthquake obtained from Spanish data. Tectonophysics 53, 301–313.

Mourabit, T., Sari, D., Reilinger, R., McClusky, S., Gomez, F., Barazangi, M., 2002. Preliminary evidence of active deformation in Morocco from repeat GPS observations. Proceedings, Wegener 2002 Conference, June 2002, Athens, Greece. abstract.

Negredo, A., Bird, P., Sanz de Galdeano, C., Buforn, E., 2002. Neotectonic modeling of the Ibero–Maghrebian region. J. Geophys. Res. 107 (B11), 2292.

Okal, E.A., 2001. "Detached" deep earthquakes: are they really? Phys. Earth. Planet. Inter. 127, 109–143.

Peacock, S.M., Wang, K., 1999. Seismic consequences of warm versus cool subduction zone metamorphism: examples from northeast and southwest Japan. Science 286, 937–939.

Pinheiro, L.M., Ivanov, M.K., Sautkin, A., Akhmanov, G., Magalhaes, V.H., Volkonskaya, A., Monteiro, J.H., Somoza, L., Gardner, J., Hamouni, N., Cunha, M.R., 2003. Mud volcanism in the Gulf of Cadiz: results from the TTR-10 Cruise. Mar. Geol. 195, 131–151.

Platt, J., Houseman, G., 2003. Comment on: Evidence for active subduction beneath Gibraltar. Geology 31 (6), e22 (Online Forum http://www.gsajournals.org/gsaonline/?request=get-static&name=i0091-7613-31-6).

Preliminary Determination of Earthquakes (PDE) Catalog (1973–present), U.S. Geological Survey, National Earthquake Information Center (NEIC), Digital Dataset available online: (http://www.neic.cr.usgs.gov).

Rehault, J.-P., Boillot, G., Mauffret, A., 1985. The western Mediterranean Basin. In: Stanley, D.J., Wezel, F.C. (Eds.), Geological Evolution of the Mediterranean Basin. Springer, Berlin, pp. 101–129.

Reilinger, R., McClusky, S., Ben Sari, D., Mourabit, T., Gomez, F., and Barazangi, M., 2001. Active deformation in Morocco from repeat GPS observations. EOS Trans. AGU, Fall Meeting 2001 Suppl. abstract.

Rimi, A., Chalouan, A., Bahi, L., 1998. Heat flow in the westernmost part of the Alpine Mediterranean system (the Rif, Morocco). Tectonophysics 285, 135–146.

Royden, L.H., 1993. Evolution of retreating subduction boundaries formed during continental collision. Tectonics 12, 629–638.

Sanchez-Rodriguez, L., Gebauer, D., 2000. Mesozoic formation of pyroxenites and gabbros in the Ronda area (southern Spain), followed by Early Miocene subduction metamorphism and emplacement into the middle crust: U–Pb sensitive high-resolution ion microprobe dating of zircon. Tectonophysics 316, 19–44.

Sandwell, D.T., Smith, W.H.F., 1997. Marine gravity anomaly from Geosat and ERS 1 satellite altimetry. J. Geophys. Res. 102, 10039–10054.

Sartori, R., Torelli, L., Zitellini, N., Peis, D., Lodolo, E., 1994. Eastern segment of the Azores–Gibraltar line (central-eastern Atlantic): an oceanic plate boundary with diffuse compressional deformation. Geology 22, 555–558.

Satake, K., 1993. Depth distribution of coseismic slip along the Nankai Trough, Japan, from joint inversion of geodetic and tsunami data. J. Geophys. Res. 98, 4553–4565.

Stampfli, G.M., Borel, G.D., Cavazza, W., Mosar, J., Ziegler, P.A., Eds., 2001. The Paleotectonic Atlas of the PeriTethyan Domain, (CD-ROM): European Geophysical Society (http://www.copernicus.org/EGS/egs_info/book.htm).

Stein, C.A., 2003. Heat flow and flexure at subduction zones. Geophys. Res. Lett. 30 (23), 2197. doi:10.1029/2003GL018478.

Stein, C.A., Stein, S., 1992. A model for the global variation in oceanic depth and heat flow with lithospheric age. Nature 359, 123–126.

Stich, D., Ammon, C.J., Morales, J., 2003. Moment-tensor solutions for small and moderate earthquakes in the Ibero–Maghreb region. J. Geophys. Res. 108, 2148.

Terrinha, P., Pinheiro, L.M., Henriet, J.-P., Matia, L., Ivanov, A.K., Monteiro, J.H., Akhmetzhanov, A., Cunha, M.R., Shaskin, P., Rovere, M., 2003. Tsunamigenic–seismogenic structures, neotectonics, sedimentary processes and slope instability on the Southwest Portuguese Margin. Mar. Geol. 3266, 1–19.

Torne, M., Fernandez, M., Comas, M.C., Soto, J.I., 2000. Lithospheric structure beneath the Alboran Basin: results from 3D gravity modeling and tectonic relevance. J. Geophys. Res. 105, 3209–3228.

Tortella, D., Torne, M., Perez-Estaun, A., 1997. Geodynamic evolution of the eastern segment of the Azores–Gibraltar Zone: the Gorringe Bank and Gulf of Cadiz region. Mar. Geophys. Res. 19, 211–230.

Watts, A.B., Platt, J.P., Buhl, P., 1993. Tectonic evolution of the Alboran Sea Basin. Basin Res. 5, 153–177.

Weinzapfel, A.C., Mountfield, R.A., Chevalier, Y.M., Kuo, L.-C., Haddad, A.C., Strickland, M.O., 2003. New insights into the hydrocarbon prospectivity of an undrilled mud diapir province, West Alboran Basin, Morocco-Spain. Proc. of Am. Assoc. Petr. Geologists Meeting, 2003. abstract.

Wells, D., Coppersmith, K., 1994. New empirical relationships among magnitude, rupture length, rupture width, rupture area and surface displacement. Bull. Seism. Soc. Am. 84, 974–1002.

Wessel, P., Smith, W.H.F., 1991. Free software helps map and display data. EOS 72, 441.

Zazo, C., Silva, P.G., Roy, J.L., Hillaire-Marcel, C., Ghaleb, B., Lario, J., Bardaji, T., Gonzalez, A., 1999. Coastal uplift in continental collision plate boundaries: data from the Last Interglacial marine terraces of the Gibraltar Strait area (south Spain). Tectonophysics 301, 95–109.

Zitellini, N., et al., 2001. Source of 1755 Lisbon earthquake and tsunami investigated. Eos (Trans., AGU) 82, 285–291.

Zitellini, N., Rovere, M., Terrinha, P., Chierici, F., Matias, L., 2004. Neogene through Quaternary tectonic reactivation of SW Iberian passive margin. Pure Appl. Geophys. 161, 565–587.